POST-MAIN SEQUENCE EVOLUTION. I: SOLAR MASS STARS

13.1 Introduction

In this and subsequent lectures, we are going to follow the evolution of stars as they progress towards the end of their lives, having concluded core hydrogen burning. The evolution is a sequence of stages which may involve nuclear burning in the core and in concentric mass shells. At various times, either core or shell burning may cease, leading to a readjustement of the internal structure of the star, with expansion or contraction of the core, and subsequent reaction of the envelope. Convection, mixing, and mass loss all play important parts.

All of these processes have been studied extensively with the aid of ever-more sophisticated computer simulations of the internal structure of stars. Unfortunately, they are too complex to be reduced to even illustrative analytical representations. So, this lecture will be largely descriptive, and our principal aim will be to explain the origin and understand the interpretation of different groups of evolved stars in the HR diagram.

As we have emphasised before, the details of the ways stars evolve off the main sequence and their ultimate fate all depend on the stellar mass. In this Lecture we consider low mass stars, with $M \sim 1M_{\odot}$. Figure 13.1 summarises the main evolutionary stages.

13.2 The Red Giant Branch

In the previous lecture, we left our solar mass star at the end of its main sequence evolution, burning H in a shell encompassing an isothermal He core. Because of the mirror action of the shell, the outer layers expand and cool and the star moves to the right in the H-R diagram. During this phase, which for a $1M_{\odot}$ star lasts $\sim 2\,\mathrm{Gyr}$, the star moves along the "*sub-*

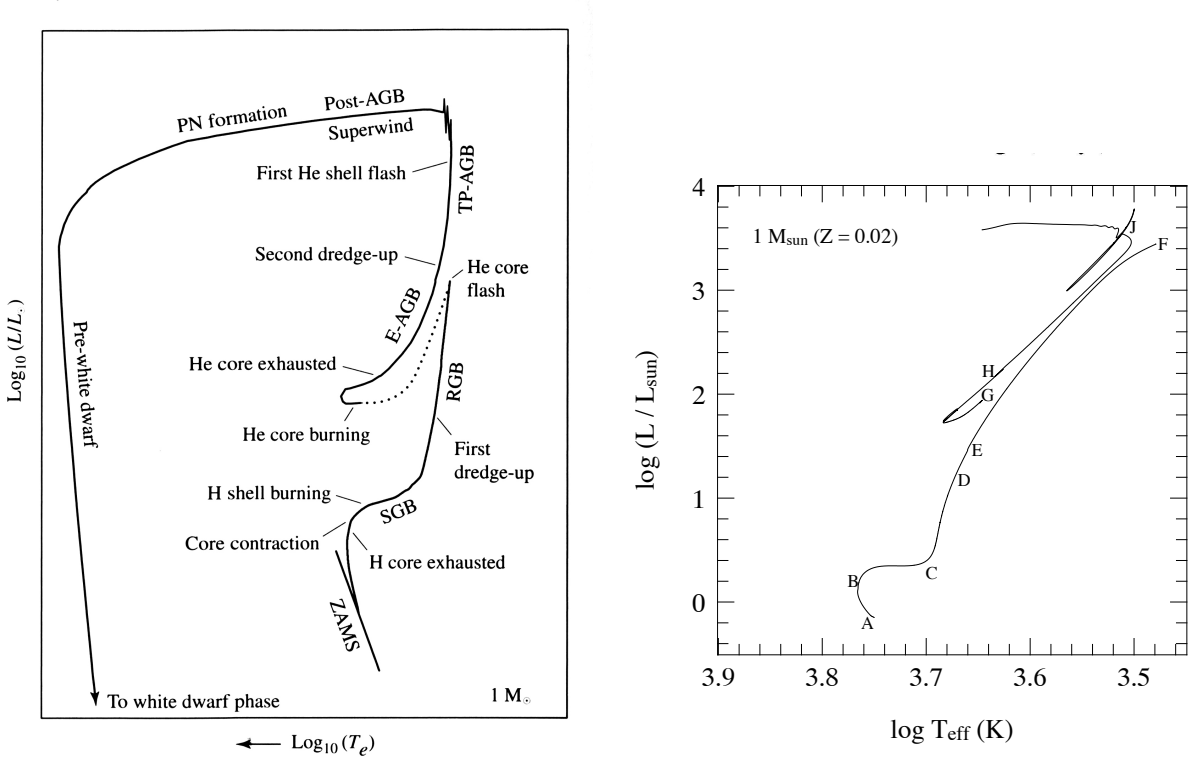

Figure 13.1: Schematic diagrams of the evolution of a $1M_\odot$ star of solar metallicity, from the main sequence to a white dwarf (*left*), and from the main sequence to a planetary nebula (*right*). The various acronyms and the lettering indicating different evolutionary stages are explained in the text.

giant branch" (SGB), between points B and C in Figure 13.1. At point C the star's He core has become degenerate.

As the star expands, however, the effective temperature cannot continue to fall indefinitely. With the expansion of the stellar envelope and the decrease in effective temperature, the photospheric opacity increases due to the additional contribution from H^- ions. When the temperature of the outer layers of the star falls below $\sim 5000\,\mathrm{K}$, they become fully convective. This enables a greater luminosity to be carried by the outer layers and hence abruptly forces the evolutionary track to travel almost vertically upwards to the *red giant branch* (RGB).

The star now moves along the same path, but in reverse, followed by a fully convective pre-main-sequence star on its approach to the main sequence, which, as we discussed in Lecture 11.7, is a nearly vertical line in the H-R diagram known as the Hayashi track. We also explained then that this track represents a boundary, in the sense that the region to the right of the track is 'forbidden': there is no mechanism that can adequately transport the luminosity out of the star at such low effective temperatures.

A $1M_\odot$ star will spend $\sim 0.5\,\mathrm{Gyr}$ on the RGB, moving from point C to point F in Figure 13.1 at an accelerating evolutionary pace, driven by what is occurring in the core. As H-fusion in the shell deposits more He onto the core, the mass of the core increases. For a fully degenerate gas, it can be shown that this results in a *contraction* of the core. As the core contracts, the density of the H-burning shell directly on top of it increases; this in turns leads to higher fusion efficiency and higher luminosity. This is a runaway process. By the end of the RGB, at point F in Figure 13.1, the degenerate He core has reached a mass of $\sim 0.5M_\odot$, and has contracted sufficiently to achieve the temperature required to ignite He fusion.

Table 13.1 Radii and Luminosities of Red Giants

	G0	G5	K0	K5	M0	M5
$\log(R/R_\odot)$	0.8	1.0	1.2	1.4	1.6	1.9
$\log(L/L_\odot)$	1.5	1.7	1.9	2.3	2.6	3.0

Table 13.1 gives some representative values for the sizes and luminosities of red giant stars; a main sequence G V star may end up as a high-K or low-M luminosity class III giant. Note that the values in Table 13.1 depend largely on the spectral type, and not on the mass: stars of a wide range of masses follow similar tracks on the RGB, becoming redder and more luminous as the core grows.

For a star with a degenerate core, the density contrast between the core and the envelope is so large that the two are practically decoupled. The pressure at the bottom of the extended envelope is very small compared to the pressure at the edge of the core and in the H-burning shell separating core and envelope. This implies that the efficiency of the shell burning is completely determined by the mass of the He core and not by the envelope. Thus, there is a strong and steep relationship between the He core mass and the luminosity of a red giant, which is entirely due to the hydrogen shell-burning source:

$$\boxed{L \simeq 2.3 \times 10^5 \left(\frac{M_c}{M_\odot}\right)^6 L_\odot} \tag{13.1}$$

Therefore, the evolutionary tracks of stars of different masses all converge onto the Hayashi line that is the RGB; from the position of a star on the RGB we can deduce the value of M_c, but the total mass is more difficult.

13.2.1 Metallicity Dependence of the RGB

The red giant branch does however exhibit a metallicity dependence. As we discussed in earlier lectures, fully convective stars are on the Hayashi line which is the locus of the lowest values of $T_{\rm eff}$ at which a star of a given luminosity can shine. Convection is related to the opacity (Lecture 8.3.1), and the opacities of stellar atmospheres depend on metallicity. This is the case even when H^- is the main source of opacity because the metals provide the free electrons that form H^-.

With a higher metallicity, an optical depth $\tau \simeq 2/3$ is reached sooner, or at lower density, as we travel from the stellar 'surface' to the core (recall the treatment of the optical depth in Lecture 5 where we took $\tau \simeq 2/3$ as

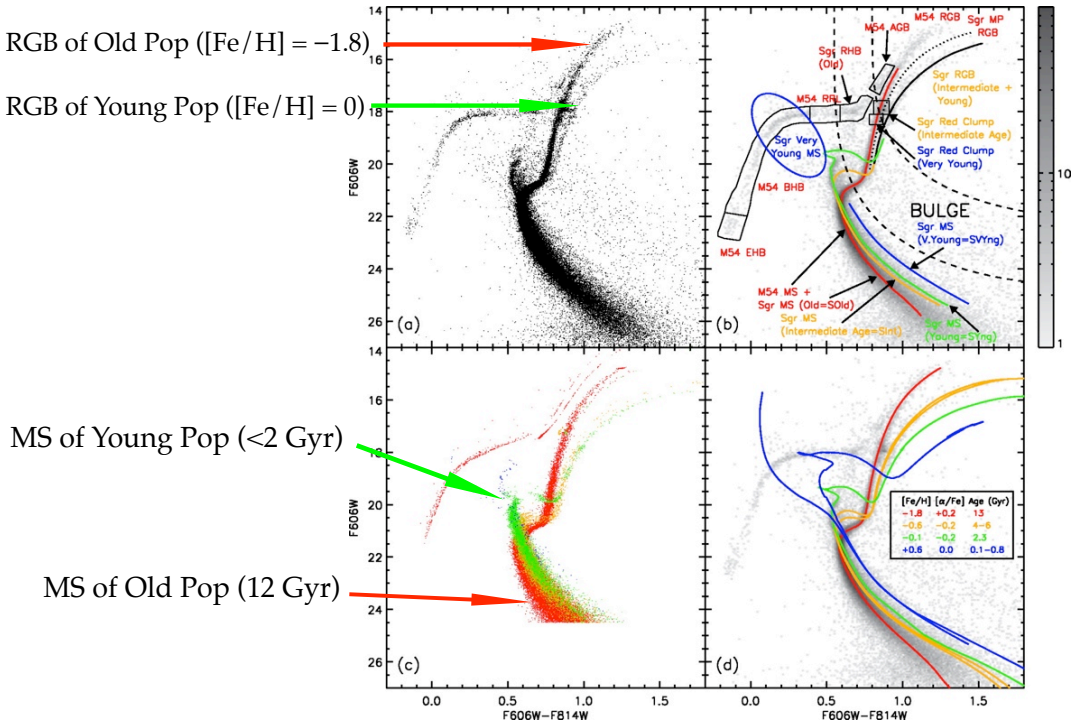

Figure 13.2: Colour-magnitude diagram (CMD) of 60 000 stars in the field of the globular cluster M54, which also includes the dwarf spheroidal galaxy Sagittarius (Sgr), which is in the process of merging with our own Galaxy. Multiple populations, of different ages and metallicities, can be distinguished in this complex CMD, allowing the past history of star formation of this companion galaxy to the Milky Way to be reconstructed. Highlighted in panel (a) are two well-separated red giant branches, whose metallicities differ by two orders of magnitude. The photometric data were measured from high spatial resolution images obtained with the Advanced Camera for Surveys on the *Hubble Space Telescope*, and published by Siegel et al. 2007, ApJ, 667, L57.

the definition of the stellar photosphere). Thus, metal-rich stars of a given mass have slightly larger radii and lower effective temperatures than stars of the same mass but lower metallicity. For the same reason, the RGB of metal-rich stars runs at slightly lower temperatures than that of metal-poor stars. A vivid demonstration is provided by the colour-magnitude diagrams of stellar systems consisting of multiple populations (see Figure 13.2).

The very steep temperature dependence of the opacity at the effective temperatures of red giants, $\kappa \propto T^9$, provides an intuitive explanation for the fact that the Hayashi line is close to vertical on a L–$T_{\rm eff}$ diagram. Suppose that a cool star of constant L could increase its radius, even by a small amount. This would lower the value of $T_{\rm eff}$ and therefore the opacity of the outer layers. As a result, we would be able to see deeper into the star, down to a depth where $\tau \simeq 2/3$, at nearly constant $T_{\rm eff}$.

13.2.2 Mass Loss on the RGB

An important process experienced by stars while they are in the red giant phase is mass loss. As the stellar luminosity and radius increase while a star evolves along the giant branch, the envelope becomes loosely bound and it is relatively easy for the large photon flux to remove mass from the stellar surface via radiation pressure (Lecture 9.2.2) on atoms and grains.

Grains are microscopic solid particles that can condense out of the gas phase at the values of temperature and pressure typical of the extended atmospheres of late-type giant and supergiant stars. Their presence in these environments is indicated by a number of infrared spectral features, such as the $9.7\,\mu$m band due to silicates, which can appear in emission or absorption in the spectra of red giants and supergiants. The winds from these stars are responsible for distributing grains into the interstellar medium, where they can subsequently grow through accretion of atoms. Interstellar grains, or *dust* as they are often referred to, are an important constituent of the diffuse interstellar medium. They regulate the heating and cooling of the ISM, act as a catalyst in the formation of H_2 molecules, and of course are responsible for interstellar extinction, the process that reddens the light of all stars.

Returning to mass loss on the RGB, red giant stars are observed to lose

mass in the form of a slow wind ($v_{\rm wind} \simeq 5$–$30\,{\rm km\ s^{-1}}$) at a rate $\dot{M} \simeq 10^{-8} M_\odot\ {\rm yr}^{-1}$. A $1M_\odot$ star loses $\sim 0.3M_\odot$ of its envelope mass by the time it reaches the tip of the giant branch.

When calculating the effect of mass loss in evolution models an empirical formula due to Reimers is often used:

$$\dot{M} = -4 \times 10^{-13}\, \eta\, \frac{L}{L_\odot}\, \frac{R}{R_\odot}\, \frac{M_\odot}{M}\ M_\odot\, {\rm yr}^{-1} \tag{13.2}$$

where the efficiency factor $\eta \simeq 0.25$–0.5. However, this relation is based on observations of only a handful of stars with well-determined stellar parameters. Note that eq. 13.2 implies that a fixed fraction of the stellar luminosity is used to lift the wind material out of the gravitational potential well of the star.

13.2.3 The First Dredge-up

As the star climbs up the RGB, its convection zone deepens until the base reaches down into regions where the chemical composition has been modified by nuclear processes. This transports processed material from the deep interior to the surface in what is referred to as the first *dredge-up* phase. This phase provides us with the first opportunity to verify empirically our ideas about nuclear burning which, up to this point, has been completely hidden from view.

For example, Li is destroyed by collisions with protons at relatively low temperatures, $T \gtrsim 2.7 \times 10^6\,{\rm K}$; as a consequence of the first dredge-up the atmospheres of evolved stars exhibit a Li deficiency compared to the Li abundance of the proto-stellar nebula. Indeed, the Li abundance is often used as a test to decide whether the atmospheric abundances can be trusted to represent the composition of the gas from which the star formed.

Similarly, the surface He abundance increases and the H abundance decreases while a star ascends the RGB. In intermediate mass stars ($M \sim 5M_\odot$), the convective envelope brings material processed by the CNO cycle to the surface. The C-N cycle reaches equilibrium before the O-N cycle, and thus CN-processed material (N enriched, C depleted) is first exposed on the surface. The N abundance increases by a factor of ~ 2, C is decreased by 30% and O is unchanged. Many red giants are observed to have

CN-processed material in their atmospheres.

13.3 The Red Giant Tip and the Helium Flash

At the tip of the RGB (point F in the right panel of Figure 13.1), the central temperature and density have finally become high enough ($T > 10^8\,\mathrm{K}$) for quantum tunnelling to overcome the Coulomb barrier between He nuclei, allowing the triple-alpha process to begin. Some of the resulting ^{12}C is further processed into ^{16}O via capture of an alpha particle (see Lecture 7.4.3). This is the onset of the helium burning phase of evolution. Unlike H-burning, the reactions involved in He-burning (Lecture 7.4.3) are the same for all stellar masses. However, the conditions in the core at the ignition of helium are very different in low-mass stars (which have degenerate cores) from stars of higher mass (with non-degenerate cores).

The electrons in the core of a $1M_\odot$ star are completely degenerate by the time the star reaches point F in Figure 13.1. Ignition in a degenerate core results in an explosive start of the fusion known as the "*Helium Flash*". The ignition of He-fusion raises the temperature of the core, but this does not raise the pressure, because in a degenerate gas $P \neq f(T)$. Thus, as T increases the core does *not* expand, and the density remains the same. As we saw in Lecture 7.4.3, the energy generation rate of the triple alpha reaction has an extraordinarily steep dependence on T: $\mathcal{E}_{3\alpha} \propto Y^3\ \rho^2\, T^{40}$. Thus, the rise in T leads to more efficient fusion, which in turn raises the T, and so on: a degenerate core that is ignited acts like a bomb!

The thermonuclear runaway leads to an enormous overproduction of energy: at maximum, the local luminosity in the helium core is $L_c \sim 10^{10} L_\odot$, comparable to the luminosity of a small galaxy! However, this only lasts for a few seconds. All the nuclear energy released is absorbed by expansion of the non-degenerate layers surrounding the core, so none of this luminosity reaches the surface. The short duration, and the presence of a very extended convective envelope that can absorb the energy created by the flash explain why the He flash has never been observed, other than in our computers (see Figure 13.3).

Since the temperature increases at almost constant density, degeneracy is eventually lifted when $T_c \simeq 3 \times 10^8\,\mathrm{K}$. Further energy release increases the

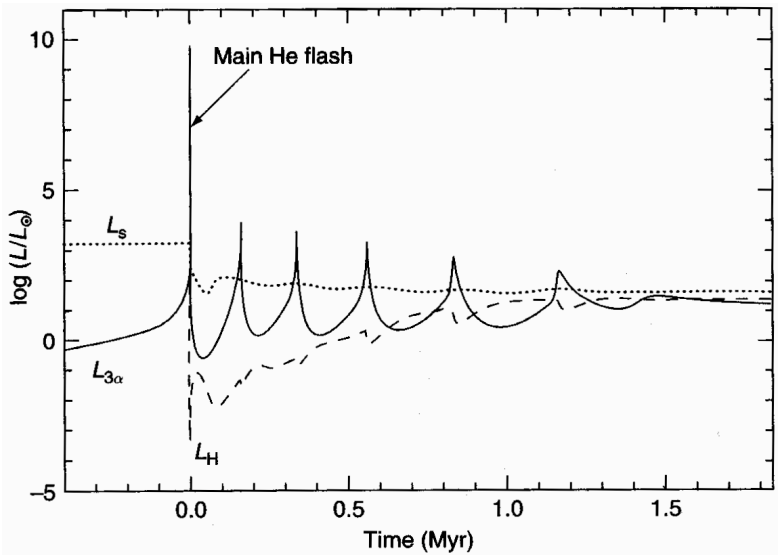

Figure 13.3: The helium flash. Evolution with time of the surface luminosity ($L_{\rm s}$), the He-burning luminosity ($L_{3\alpha}$) and the H-burning luminosity ($L_{\rm H}$) during the onset of He burning at the tip of the RGB in a low-mass star. Time $t = 0$ corresponds to the start of the main helium flash. (Figure from Salaris & Cassisi, Evolution of Stars and Stellar Populations, Wiley).

pressure when the gas starts behaving like an ideal gas and thus causes expansion and cooling. This results in a decrease of the energy generation rate until it balances the energy loss rate and the core settles in thermal equilibrium at $T_c \simeq 10^8\,{\rm K}$. Further nuclear burning is thermally stable.

After the He flash, the whole core expands somewhat but remains partially degenerate. In detailed models, a series of smaller flashes follows the main He flash (see Figure 13.3) for $\sim 1.5\,{\rm Myr}$, before degeneracy in the centre is completely lifted and further He burning proceeds stably in a convective core.

This is the situation when stars with a *non-degenerate* core reach $T_c \sim 10^8\,{\rm K}$ at the tip of the RGB. In this case, the rise in T_c is accompanied by an increase in P. The core expands, T_c and P decrease, the energy production drops, and the core shrinks until it reaches hydrostatic equilibrium again. So, in this case, gravity acts like a regulator and the star does not experience a He flash. The dividing line between stars with degenerate and non-degenerate cores at the tip of the RGB is $\sim 2M_\odot$; stars with $M \lesssim 2M_\odot$ undergo a He flash, while in those with $M \gtrsim 2M_\odot$ He burning is ignited without a thermonuclear runaway event.

13.4 The Horizontal Branch

In our $1M_\odot$ star, the He flash occurs at point F in Figure 13.1. Evolution through the helium flash was not calculated for the model shown in this figure, because the evolution is very fast and hard to follow. The evolution of the star is resumed at point G when the star has settled into a new equilibrium configuration with an expanded non-degenerate core which is hot enough to burn He. The star now has two sources of energy generation: core He fusion and shell H fusion. However, the H-burning shell has also expanded and now has lower temperature and density; consequently, it generates less energy than when the star was at the upper end of the RGB. The lower total luminosity is insufficient to keep the star in its distended red giant state; the star shrinks in size, dims and settles on the *horizontal branch*.

At this point the luminosity and radius of the star have decreased by more than one order of magnitude from their values just before the He flash. Here we again see the mirror principle at work: in this case the core has expanded (from a degenerate to a non-degenerate state) and the envelope has simultaneously contracted, with the H-burning shell acting as a mirror.

The horizontal branch is the core He-burning equivalent of the core H-burning main sequence. However, while a $1M_\odot$ star spends $\sim 1 \times 10^{10}\,\mathrm{yr}$ on the main sequence, its core He-burning phase on the HB lasts only $\sim 120\,\mathrm{Myr}$, or $\sim 1\%$ of its main sequence lifetime, because of the much higher luminosity of the He-burning phase.

13.4.1 The Horizontal Branch Morphology

For the $1M_\odot$ star of solar composition considered in Figure 13.1, He burning occurs between points G and H. The location of the star in the H-R diagram does not change very much during this period, always staying close to (but somewhat to the left of) the red giant branch. Its luminosity is $\sim 50L_\odot$ for most of the time, a value determined mainly by the core mass. Since the core mass at the start of helium burning is $\sim 0.45M_\odot$ for all low-mass stars, irrespectively of stellar mass, the luminosity at which He burning occurs is also almost independent of the total stellar mass. Thus, it is only the

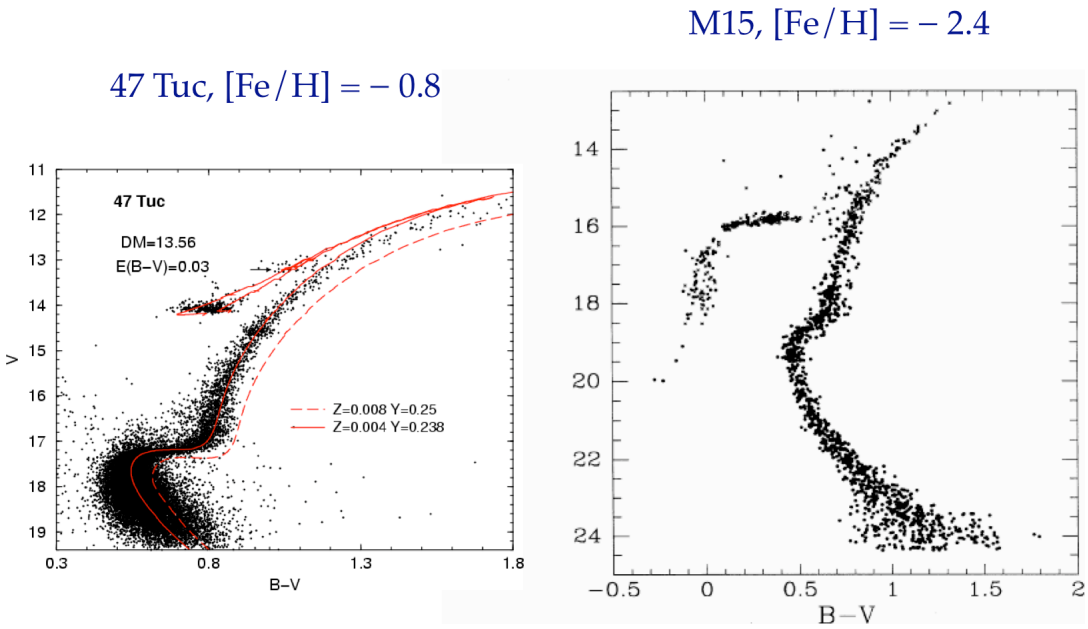

Figure 13.4: The Fe abundances of the stars in these two Galactic globular clusters differ by a factor of ~ 40. In the more metal-poor globular cluster, M15 on the right, the horizontal branch extends much further to the blue (hotter effective temperatures, implying smaller radii) than in the more metal-rich one (47 Tuc, on the left).

envelope mass that varies from star to star, either because of differences in mass on the ZAMS, or as a result of different amounts of mass loss on the RGB.

At solar metallicity, all core He-burning stars occupy a similar locus in the H-R diagram, which is referred to as the '*red clump*'. However, in metal-poor globular clusters these stars are found to be spread out over a range of effective temperatures at the same approximate luminosity—hence the *'horizontal branch'* nomenclature. It is thought that the location of a star on the HB is a reflection of its envelope mass: stars with smaller envelopes (and hence radii) are bluer (and are therefore found on the left of the HB).

The extent of the horizontal branch in globular clusters seems to be related to their metallicity. The more metal-rich globular clusters tend to have a red HB, while in the more metal-poor ones the HB extends further to the blue (see Figure 13.4). In this respect, the red clump of solar metallicity stars may be simply the red extreme of the HB. But metallicity is not the only factor at play here, because there are known cases of globular clusters with a blue HB and others with a red HB even though their metallicities are similar! This has led astronomers to invoke a 'second parameter', a label that acknowledges that some other unknown physical effect is responsible for HB morphology differences in clusters that seem to be very similar in most of their physical properties. Age, He content and rotation have been

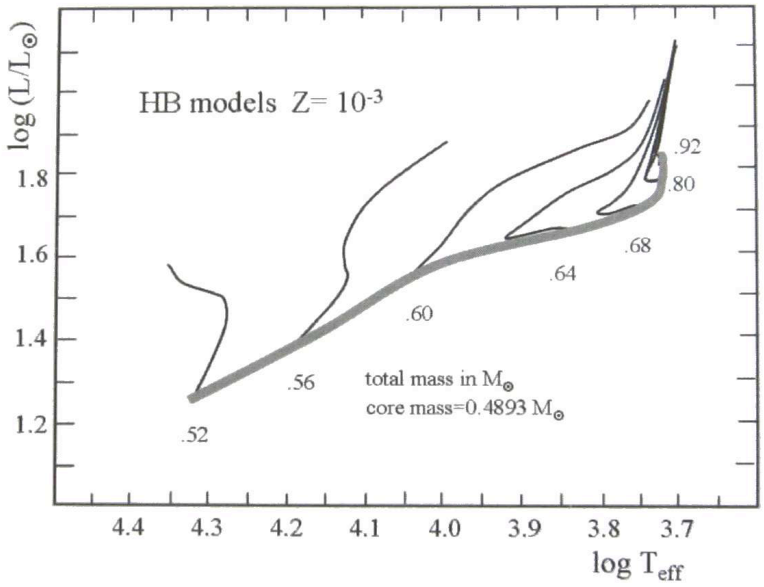

Figure 13.5: Location of the zero-age horizontal branch (thick grey line) for a metallicity $Z = 0.001$ which is typical of Galactic globular clusters. The models shown all have the same core mass ($M_c = 0.489 M_\odot$) but varying total (i.e. envelope) mass, which determines their position in the H-R diagram. Evolution tracks during the HB phase for several total mass values are shown as thin solid lines. (Figure from Maeder, A., Physics, Formation and Evolution of Rotating Stars, Springer-Verlag).

proposed, but the underlying cause of different HB morphologies remains a long-standing problem in stellar astrophysics.

Once a star has entered the HB (on the left, the right or in between), evolution moves it to the right during the core He fusion phase, due to the increasing depth of the convection zone (see Figure 13.5).

13.5 The Asymptotic Giant Branch (AGB)

Returning to Figure 13.1, by the time the star has reached stage H, it has exhausted its supply of He in the core which now consists of C and O. The core contracts again, but in stars with masses $M < 8M_\odot$ there is insufficient gravitational energy to generate the high temperatures required to fuse C and O into heavier nuclei. Thus, no more core fusion takes place in these stars. However, the core contraction generates sufficient heat for the surrounding layer of He to start fusing in a shell.

The next phase of the evolution is very similar to the evolution we have already discussed following exhaustion of the hydrogen burning core. The contraction of the core leads to a strong expansion of the star's outer

layers, causing its surface temperature to drop and moving the star to the right and upwards in the H-R diagram along the *Asymptotic Giant Branch* (AGB). A $1M_{\odot}$ AGB can reach a luminosity $L \sim 10^5 L_{\odot}$! The AGB is so named because the evolutionary track approaches the line of the RGB asymptotically from the left, and indeed it can be thought of as the shell He-burning analogue of the shell H-burning RGB. At solar metallicities the AGB lies close to the RGB, but in metal-poor globular clusters the AGB and RGB appear well separated.

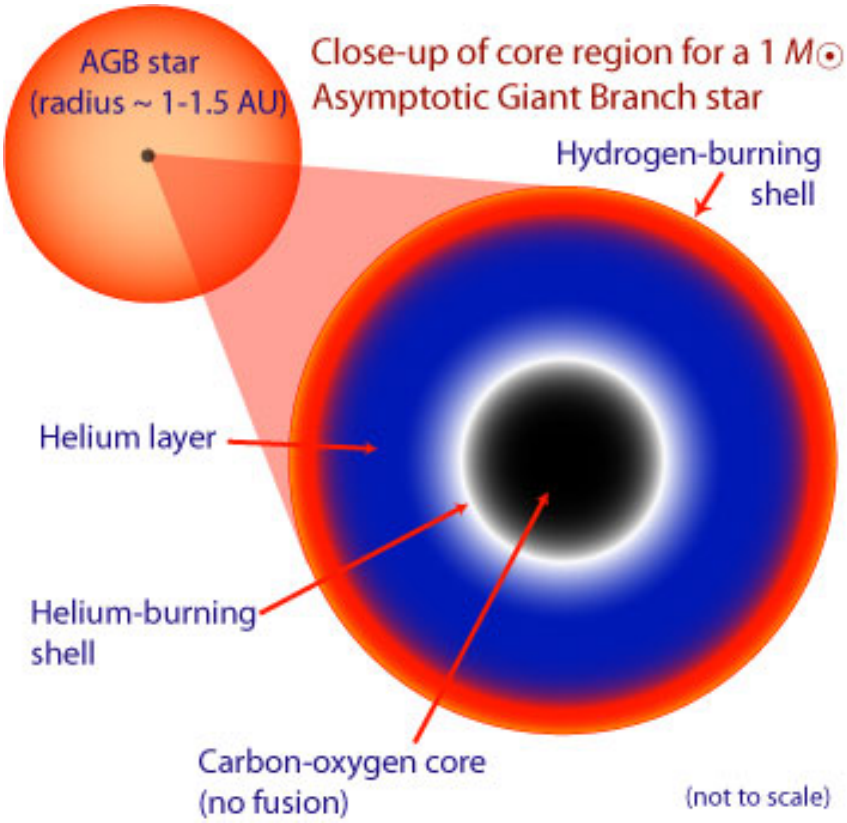

Figure 13.6: Schematic structure of a solar mass star during the RGB phase.

A this point, the star consists of: (i) a degenerate C+O core; (ii) a He-burning shell; (iii) an inert He-shell around it; (iv) a H-burning shell; and (v) an outer H-rich convective envelope (see Figure 13.6).

The evolution is now complex because the huge differences between the two nuclear fusion processes do not allow a steady state to exist. The two shells supply the luminosity of the AGB star alternately in a cyclical process, or a thermal pulsation, which has a period of $\sim 1000\,\mathrm{yr}$, with the changes triggered by shell flashes.

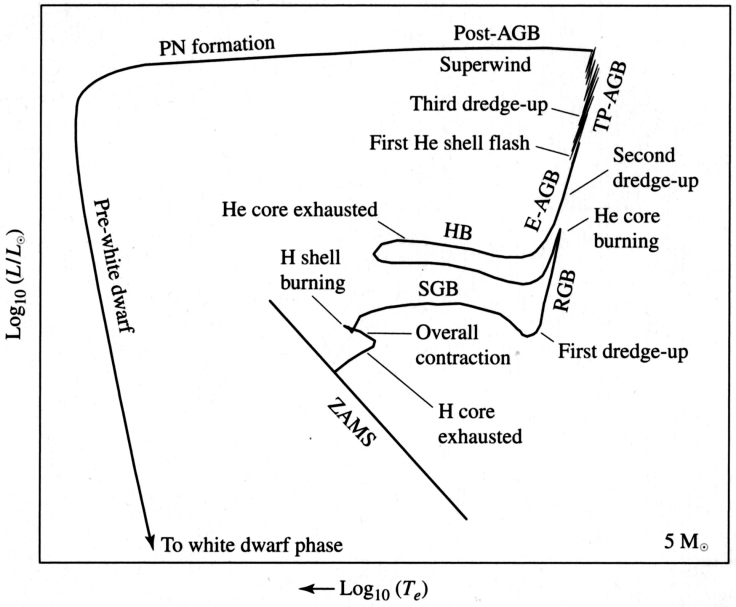

Figure 13.7: Schematic diagram of the evolution of a $5M_\odot$ star of solar metallicity, from the main sequence to a white dwarf.

Although brief (a $1M_\odot$ star will spend $\sim 5\times10^6$ yr on the AGB), the AGB is an interesting and important phase of stellar evolution. The expansion and cooling of the envelope increase its opacity and the depth of the convection zone which can reach down to the chemical discontinuity between the H-rich outer layer and the He-rich region between the two burning shells. The mixing that results during this *second dredge-up* phase increases the He and N content of the envelope.

In stars more massive than $\sim 2M_\odot$, there a *third dredge-up* as the tip of the AGB is approached, driven by thermal pulsations (see Figure 13.7). This brings to the surface C-rich material and 's-process' elements (see later) In stars more massive than $\sim 3M_\odot$, the base of the convective envelope becomes hot enough for the CN cycle to operate and the dredged-up C is converted to N, in a process called 'hot bottom burning'.

At the low temperatures of the atmospheres of AGB stars, most of the C and O atoms are bound into CO molecules, since this is the most stable molecule. In the protostellar nebula, C/O ~ 0.5 (see Figure 6.13). If this initial abundance has not been changed appreciably and all the C is locked in CO molecules, then the remaining O atoms form oxygen-rich molecules and dust particles, such as TiO, H_2O and silicate grains. The spectra of such O-rich AGB stars are classified as type M or S. However, as a result of repeated dredge-up events, at some point the C/O ratio can exceed

unity. In this case all O is locked into CO molecules and the remaining C forms carbon-rich molecules and dust grains, e.g. C_2, CN, C_nH_n, and carbonaceous grains like graphite and SiC. Such more evolved AGB stars are classified as carbon stars with spectral type C. Besides carbon, the surface abundances of many other elements and isotopes change during the Thermal-Pulse (TP) AGB phase.

13.5.1 Slow Neutron Capture Nucleosynthesis

Direct evidence for active nucleosynthesis in AGB stars was provided in 1953 by the detection of technetium ($_{43}$Tc), the lowest atomic number element *without* any stable isotopes: every form of it is radioactive. The longest lived isotope, $^{99}_{43}$Tc, decays on a timescale of only 2×10^5 yr. Spectroscopic observations actually show that many AGB stars are enriched in elements heavier than iron, such as Zr, Y, Sr, Tc, Ba, La and Pb. These elements are produced via slow neutron capture reactions on Fe nuclei, the s-process which we have already discussed in Lecture 7.5. In this context slow means that the time between successive neutron captures is long compared to the β-decay timescale of unstable, neutron-rich isotopes. The synthesis of s-process elements requires a source of free neutrons, which can be produced in the He-rich intershell region by a number of reactions. AGB stars are nowadays considered to be major producers in the Universe of carbon, nitrogen and of elements heavier than iron synthesised via the s-process. They also make an important contribution to the production of ^{19}F, ^{25}Mg, ^{26}Mg and other isotopes.

13.5.2 Mass loss and the post-AGB phase

During the AGB phase, the mass loss increases dramatically from $\dot{M} \simeq 10^{-8}$ to $\simeq 10^{-4} M_\odot$ yr^{-1}. We can easily see this:

$$\frac{dM_{\rm star}}{dt} = -\frac{dM_{\rm wind}}{dt}\,, \tag{13.3}$$

and

$$\frac{dM_{\rm env}}{dt} = -\frac{dM_{\rm wind}}{dt} - \frac{dM_{\rm core}}{dt}\,. \tag{13.4}$$

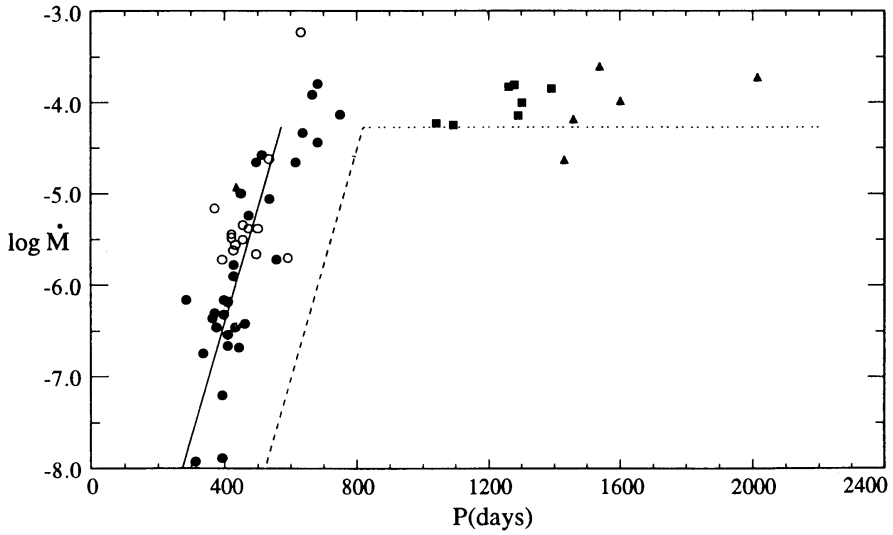

Figure 13.8: Mass loss of AGB stars. The observed correlation between the pulsation period P of Mira variables and their mass-loss rate $\dot{M}$, in $M_\odot$ yr^{-1}. (Figure reproduced from Vassiliadis & Wood 1993, ApJ, 413, 641).

But:

$$\frac{dM_{\rm wind}}{dt} = f(L) \tag{13.5}$$

(see eq. 13.2), and

$$L = f(M_{\rm core}) \tag{13.6}$$

In fact, mass loss becomes so strong on the AGB that the entire H-rich envelope can be removed before the core has had time to grow significantly. The lifetime of the TP-AGB phase, $t_{\rm TP-AGB} \sim 1$–2×10^6 yr, is essentially determined by the mass-loss rate.

The high mass-loss rate distributes the chemical elements and dust grains found in the outer atmospheres of AGB stars into the surrounding interstellar medium. Many AGB stars (known as OH/IR stars) are completely enshrouded in a dusty circumstellar envelope which renders them invisible at optical wavelengths. The mechanisms driving such strong mass loss are not fully understood, but it is likely that both dynamical pulsations and radiation pressure on dust particles play a role.

AGB stars undergoing strong radial pulsations are known as 'Mira variables'. Observationally, a correlation is found between the pulsation period and the mass-loss rate, shown in Figure 13.8. As a star evolves towards larger radii along the AGB, the pulsation period increases and so does the mass-loss rate, from $\dot{M} \sim 10^{-8}$ to $\sim 10^{-4} M_\odot$ yr^{-1} for pulsation periods in excess of about 600 days. This phase of very strong mass loss is sometimes

called a 'superwind'. Once an AGB star enters this superwind phase, the H-rich envelope is rapidly removed marking the end of the AGB phase. The high mass-loss rate during the superwind phase therefore determines both the maximum luminosity that a star can reach on the AGB, and its final mass, i.e. the mass of the white-dwarf remnant.

The mass loss rate increases until the mass of the remaining envelope has reached some minimum value, 10^{-2}–$10^{-3} M_\odot$, such that a convective envelope can no longer be sustained and the envelope starts to contract into radiative equilibrium and the star leaves the AGB. The resulting decrease in stellar radius occurs at almost constant luminosity, because the H-burning shell is still fully active and the star keeps following the core mass-luminosity relation. The star thus follows a horizontal track in the H-R diagram towards higher effective temperatures. This is the *post-AGB* phase of evolution. Note that the star remains in complete equilibrium during this phase: the evolution towards higher $T_{\rm eff}$ is caused by the decreasing mass of the envelope, which is eroded at the bottom by H-shell burning and at the top by continuing mass loss. The typical timescale for this phase is $\sim 10^4$yr.

13.6 Planetary Nebulae

As the star gets hotter and $T_{\rm eff}$ exceeds 30 000 K, two effects come into play: (1) the star develops a weak but fast wind ($\dot{M} \simeq 10^{-6} M_\odot$ yr^{-1}, $v_{\rm exp} \simeq 1000$ km s^{-1}), driven by radiation pressure in UV absorption lines (similar to the winds of massive OB-type stars which we shall discuss in a subsequent lecture); and (2) the strong UV flux destroys the dust grains in the circumstellar envelope, dissociates the molecules and finally ionizes the gas. Part of the circumstellar envelope thus becomes ionized (an H II region) and starts radiating in recombination lines: a young *Planetary Nebula* (PN) is born. (PNs have nothing to do with planets, of course. The name has its origin in the fact that, like planets, they are not point-like sources, and therefore did not appear to 'twinkle' due to atmospheric turbulence when observed with the naked eye by early astronomers. The misnomer has stuck).

For a long time it was believed that the PN represented the previous AGB

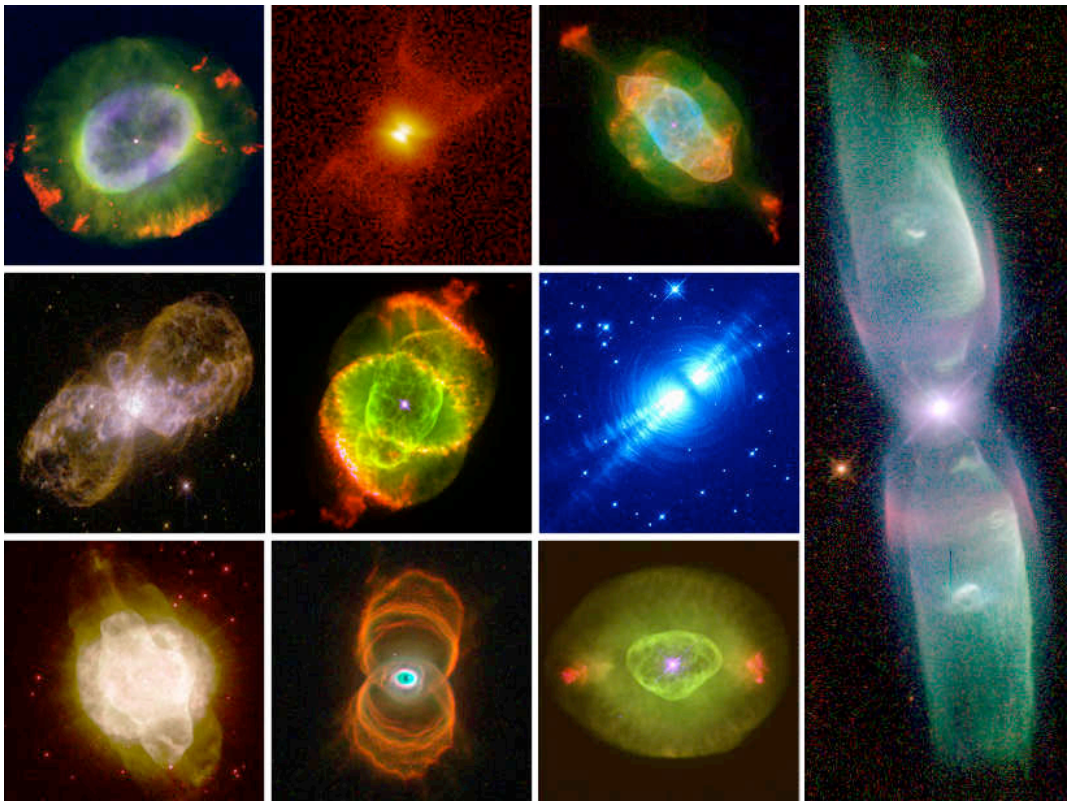

Figure 13.9: Images of Planetary Nebulae taken with the *Hubble Space Telescope*.

wind. However, a puzzled remained: the observed expansion speeds of PNs are typically $v_{\rm exp} \simeq 50\,{\rm km\ s^{-1}}$, whereas AGB winds are ejected with much lower velocities, only 10–15 km s^{-1}. How could the AGB material be accelerated? However, once it was realised (in 1975) that the central stars of PNs have fast stellar winds, then the current scenario was proposed (by Sun Kwok and collaborators): planetary nebulae result from the interaction between the slow AGB wind and the fast wind from the central star. The fast wind sweeps up and accelerates the AGB wind, forming a compressed optically thin shell from which the radiation is emitted.

Images of Planetary Nebulae taken with the *Hubble Space Telescope* reveal a wide variety of often very complex shapes (see Figure 13.9). Bruce Balick (1987, AJ, 94, 671) put forward an empirical morphological classification of PNs, ranging from spherical, through elliptical, to 'butterfly', and proposed that these different morphologies result from spherical asymmetries in the wind of the AGB progenitor. According to his suggestion, a relatively moderate density contrast in the slow AGB wind between the equatorial and polar directions produces an elliptical shell, while a strong contrast results in a 'butterfly' shape. Such a density contrast may be related to rotation. Soker & Livio (1989, ApJ, 339, 268) extended this idea to PNs

containing binary nuclei. Here common envelope evolution of the binary system can naturally produce the density contrast between the equatorial (orbital) plane and polar directions upon which the interacting wind model can operate. Some of the more complex PN morphologies may be due to the influence of magnetic fields.

13.6.1 The spectra of planetary nebulae

The diffuse gases which constitute a planetary nebula are heated and ionised by the hard UV radiation emitted by the hot central star with $T_{\rm eff} = 30\,000$–$100\,000$ K. Recalling the discussion in Lecture 3 (Figure 3.1), the nebula will emit a spectrum which is dominated by emission lines, with very little or no continuum; an example is reproduced in Figure 13.10.

The strongest emission lines are H and He recombination lines, emitted following capture of free electrons by ionized H and He atoms, and collisional lines excited by inelastic electron impacts with heavy elements ions. The latter are usually indicated with square brackets because they are 'forbidden' transitions, by which we mean that they cannot proceed via the most efficient (electric dipole) route, and thus have much lower transition

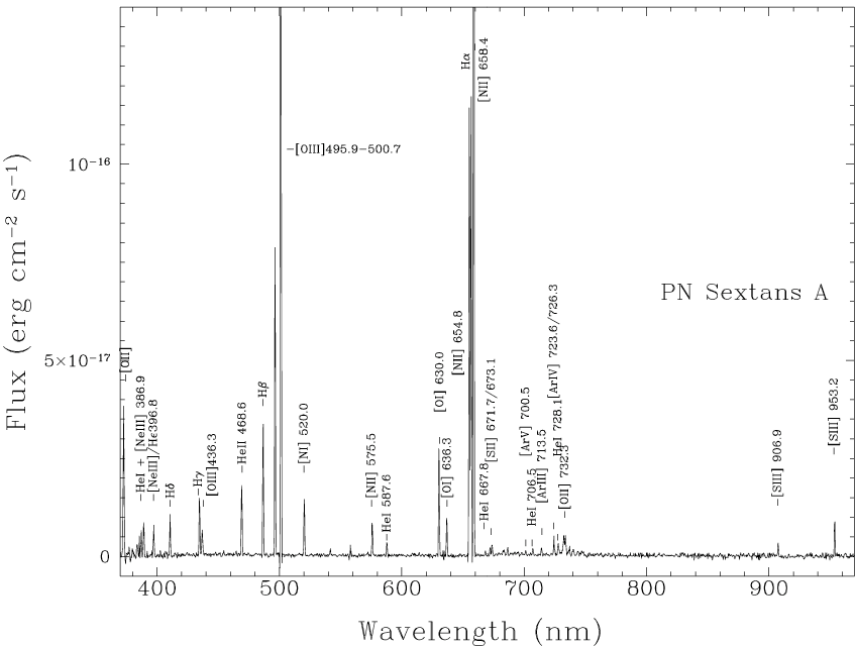

Figure 13.10: Emission line spectrum of a Planetary Nebula recorded with the Very Large Telescope of the European Southern Observatory at Cerro Paranal, Chile. (Figure reproduced from Magrini et al. 2005, A&A, 443, 115).

probabilities than transitions allowed by the selection rules of quantum mechanics.

These emission lines are a veritable treasure-trove of information on the physical conditions within the nebula; from their relative strengths it is possible to deduce values of the electron temperature and density, as well as the relative abundances of different elements. Planetary nebulae have played a key role in the development of nebular diagnostic techniques. They are one of the best astrophysical laboratories for studying the physical processes operating within ionized nebulae in general, and for testing the atomic data that are central to stellar and nebular models.

Because their spectra are dominated by strong and narrow emission lines, PNs can be recognised in external galaxies a distances where individual stars are too faint to be detected. An extra bonus is that their radial velocities can be measured very precisely. These characteristics have been exploited in the recently developed 'Planetary Nebula Spectrograph', an instrument especially designed with the goal in mind of using PNs as probes of galaxy kinematics. Specifically, by measuring the projected velocities of large numbers of PNs within a single elliptical galaxy, it is possible to reconstruct its gravitational potential, and thereby probe the distribution of both luminous and dark matter. Traditionally, this has only been possible in gas-rich spiral galaxies via the 21 cm emission line of neutral hydrogen. Elliptical galaxies, on the other hand, have little gas left, so that alternative strategies had to be devised.

The distribution of [O III] λ5007 emission line strengths in PNs appears to have a sharp bright-end cut-off. This has led to attempts to use PNs as 'standard candles' in determining cosmological distances.

`http://web.williams.edu/astronomy/research/PN/nebulae/` is a great site for further images, spectra and general information on PNs.

13.7 White Dwarfs

When the stellar envelope mass has decreased to $10^{-5} M_{\odot}$, the H-burning shell is finally extinguished and from this point on the luminosity of the star decreases as it cools from $T_{\rm eff} \simeq 10^5\,{\rm K}$. All stars with initial masses

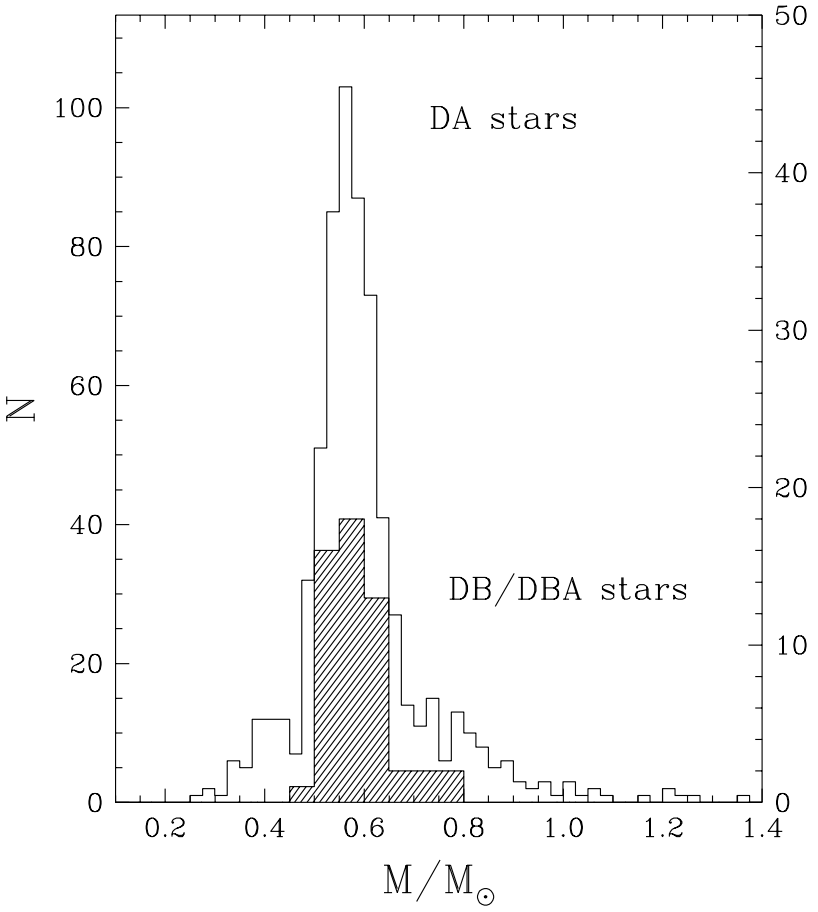

Figure 13.11: Observed mass distribution of white dwarfs, for a large sample of DA white dwarfs and a smaller sample of DB white dwarfs. In both samples, there is a sharp peak between $M = 0.55M_\odot$ and $0.6M_\odot$, as expected if most white dwarfs come from low-mass progenitors with masses $M_{\rm ZAMS} \leq 2M_\odot$. (Figure reproduced from Bergeron et al. 2007, ASPC, 372, 29).

$M_{\rm ZAMS} \lesssim 8M_\odot$, develop electron-degenerate cores, lose their envelopes during the AGB phase, and end their lives as white dwarfs (WD). Nuclear fusion no longer provides energy: white dwarfs shine by radiating the thermal energy stored in their interiors, cooling at almost constant radius and decreasing luminosity. The faintest white dwarfs detected have $L \approx 10^{-4.5}L_\odot$. Observed WD masses are mostly in a narrow range around $\sim 0.6M_\odot$ (see Figure 13.11), which corresponds to the CO core mass of low-mass ($M_{\rm ZAMS} \lesssim 2M_\odot$) AGB progenitors. This sharply peaked mass distribution is further evidence that AGB mass-loss is very efficient at removing the stellar envelope.

We shall return to White Dwarfs in a subsequent lecture.

13.8 Summary

Table 13.2 summarises the timescales relevant to the different evolutionary stages of a $1M_\odot$ star.

Table 13.2 Approximate Timescales in the Evol. of a $1M_\odot$ Star

Phase	t (yr)
Main Sequence	1×10^{10}
Subgiant	2×10^{9}
Red Giant Branch	5×10^{8}
Horizontal Branch	1×10^{8}
Asymptotic Giant Branch	5×10^{6}
Planetary Nebula	1×10^{5}
White Dwarf (cooling)[a]	$> 8 \times 10^{9}$

Notes:

[a] Age of the Galactic disk.